frontiers | Frontiers in Detector Science and Technology

TYPE Methods
PUBLISHED 28 April 2025
DOI 10.3389/fdest.2025.1488822

OPEN ACCESS

EDITED BY
Florian Brunbauer,
European Organization for Nuclear Research (CERN), Switzerland

REVIEWED BY
Francesc Monrabal Capilla,
Donostia International Physics Center (DIPC), Spain
Douglas Bryman,
University of British Columbia, Canada

*CORRESPONDENCE
Min Zhong,
mizhong@ucsd.edu

RECEIVED 30 August 2024
ACCEPTED 07 April 2025
PUBLISHED 28 April 2025

CITATION
Backues A, Feng J, Ni M and Zhong M (2025) Design of a high-resolution liquid xenon detector for positron emission tomography. *Front. Detect. Sci. Technol.* 3:1488822.
doi: 10.3389/fdest.2025.1488822

Design of a high-resolution liquid xenon detector for positron emission tomography

Alexander Backues[1], Jeremy Feng[2], Matthew Ni[1] and Min Zhong[3]*

[1]Canyon Crest Academy, San Diego, CA, United States, [2]The Bishop's School, La Jolla, CA, United States, [3]Department of Physics, University of California, San Diego, La Jolla, CA, United States

Positron Emission Tomography (PET) is a vital imaging technique extensively used for early cancer detection by visualizing metabolic processes in the body. While traditional PET systems use scintillation crystals like bismuth germanate (BGO) or lutetium oxyorthosilicate (LSO) to detect gamma rays, they have inherent energy and spatial resolution limitations. This paper proposes an advanced PET design using liquid xenon (LXe)-based detectors that integrate scintillation and ionization energy detection. Our PET detector design has a monolithic liquid xenon target of $5 \times 5 \times 5\,\mathrm{cm}^3$, from where scintillation light is detected by silicon photomultipliers (SiPMs) placed on one side of the target. The ionization is converted to field-enhanced electroluminescence in liquid xenon and detected by the same SiPMs. We use Monte Carlo simulations to optimize the configuration of the electric field and improve the light collection efficiency. Combining both detection modes, the proposed system aims to significantly improve the energy resolution to approximately 2% full width at half maximum (FWHM). Furthermore, machine learning models enhance position reconstruction accuracy with sub-millimeter horizontal and depth-of-interaction (DOI) resolutions. The results indicate that the LXe-based PET detector can achieve superior performance compared to current PET technologies, offering enhanced imaging accuracy with the potential for reduced doses of radioactive tracer.

KEYWORDS

liquid xenon detector, electroluminescence, positron emission tomography, energy resolution, position resolution

1 Introduction

1.1 Positron emission tomography (PET)

Positron Emission Tomography (PET) is a vital imaging technique used in the medical industry to detect metabolic and biochemical activity in tissues, particularly for diagnosing and monitoring conditions such as cancer, neurological disorders, and cardiovascular diseases. As a billion dollar industry, PET scans can frequently identify abnormal tracer metabolism in diseases before they become apparent on other imaging tests, making them a valuable asset to the medical world (Mordor Intelligence, 2024).

The core technology of Positron Emission Tomography (PET) scans leverages subatomic physics to produce three-dimensional images of a patient's body (Berg and Cherry, 2018), Initially, a small amount of radioactive material, typically fluorine-18 labeled glucose, is introduced into the patient's body as a radioactive tracer (Alauddin, 2012). This tracer emits positrons, positively charged subatomic particles that interact with electrons in areas of a patient's body with high blood density. Through the process of positron-electron annihilation, a positron encounters an electron. It simultaneously produces two high-energy photons, each measuring 511 keV, traveling in opposite directions in a straight line. These photons are detected by a ring of detectors surrounding the patient. Using time-of-flight (TOF) techniques, which measure the difference in the time it takes for the photons to reach the detectors, the system can improve the reconstruction of the origin of the photons. The PET constructs a detailed image of the body's metabolic activity, allowing doctors to pinpoint areas of abnormal function, such as cancerous growths.

Optimizing the detection of 511 keV gamma rays is a critical aspect of PET technology, crucial for improving the accuracy and resolution of scans. Modern PET systems rely on scintillation crystals, typically made of materials like bismuth germanate (BGO), lutetium oxyorthosilicate (LSO), or lutetium-yttrium oxyorthosilicate (LYSO), to detect gamma-ray energy (Vallabhajosula, 2023). When a 511-keV gamma-ray interacts with a scintillation crystal, it deposits energy through photoelectric effect or Compton scattering. The absorbed energy excites electrons in the crystal's lattice, raising them to higher energy states. As these electrons return to their ground state, they emit photons in the visible or near-UV range. The number of emitted scintillation photons is proportional to the deposited energy. These emitted scintillation photons are collected by a photodetector, typically a photomultiplier tube (PMT) or silicon photomultiplier (SiPM). The photodetector signals are then processed to determine the location and energy of the detected gamma-ray, which contributes to reconstructing the PET image.

The industry standard for scintillation crystal energy resolution is typically 10% FWHM (full width at half maximum) and spatial and DOI (depth-of-interaction) resolutions of 2–3 mm (Berg and Cherry, 2018). Our objective is to significantly enhance the energy and spatial resolutions of individual PET detectors, thereby improving the overall performance of the PET imaging system.

1.2 Liquid-xenon based PET detectors

The challenge of achieving high-resolution gamma-ray detection is not confined solely to medical imaging; it also plays a crucial role in fields like dark matter detection and neutrino physics. Significant research and optimization efforts have been dedicated to enhancing the sensitivity and efficiency of detectors in these areas. A prime example is the XENON1T detector, located at the Gran Sasso National Laboratory in Italy, which is designed to detect Weakly Interacting Massive Particles (WIMPs), a leading dark matter candidate. This detector utilizes scintillation detection technology and employs electric fields to detect ionization energy, thereby improving its energy resolution (Aprile et al., 2020). Similarly, advanced detector technology is employed in the EXO experiment to search for the neutrinoless double beta decay of isotope Xe-136 (Anton et al., 2020). These technologies underscore the critical importance of high-resolution detection across multiple domains in fundamental physics.

Our project aims to develop an alternative PET design that replaces the traditional scintillation crystal technology with a Liquid Xenon (LXe)-based detection system, enhancing data accuracy and precision. The concept of using LXe in PET scans is not entirely new; a multiwire ionization chamber with LXe was used for PET development by Chepel et al. (1999), time-of-flight PET system utilizing LXe to achieve high timing resolution was proposed by Doke et al. (2006) and the PETALO project (Romo-Luque, 2020). However, their design features a uniform ring filled with LXe without incorporating ionization energy detection via an electric field. Simultaneous reconstruction of scintillation light and ionization charge produced by 511 keV photons in liquid xenon for potential application to PET has been investigated in the past (Giboni et al., 2007; Amaudruz et al, 2009; Miceli et al., 2011). Another LXe medical imaging system, named XEMIS2, utilizes both scintillation and ionization for reconstructing the source positions as a Compton camera (Manzano et al., 2018). Our design aims for sub-nanosecond timing precision, comparable to PETALO (Romo-Luque, 2020). In addition, we seek to further improve the energy and spatial resolutions of individual PET detectors by using both scintillation and ionization-induced electroluminescence readout to push the boundaries of imaging performance.

Detecting scintillation (photon) and ionization (electron) energy allows us to reconstruct the total energy that deposits into liquid xenon. Such an improved energy resolution by combining the two signals was demonstrated in particle physics and is now widely used in dark matter and neutrino research, such as in the EXO experiment (Anton et al., 2020) and in the LZ dark matter search experiment (Pereira et al., 2023).

This project aims to show that a liquid xenon detector with both scintillation and ionization detection will significantly increase the energy and position resolutions, including the depth-of-interaction (DOI) information. We first present the detection principle and the detector design in Section 2. Detailed Monte Carlo simulations are performed and results are presented in Section 3 to show the light and electron detection efficiencies of the proposed liquid xenon detector design, and its achievable energy resolutions. In Section 4, we present position resolution results based on two machine learning reconstruction models.

2 Detector design

The cryogenic and purification systems to maintain a stable operation of the LXe detector have been developed in the particle physics field and many have become standard technology. For example, the pulse tube refrigerator used in the XENON1T dark matter detector (Aprile et al., 2017) provides 250 W cooling power at the LXe temperature around $-96^{o}C$. Unlike the dark matter detector, the LXePET system does not require low background materials but the liquid xenon itself needs to be constantly circulated with a pump and purified through a getter, such as the

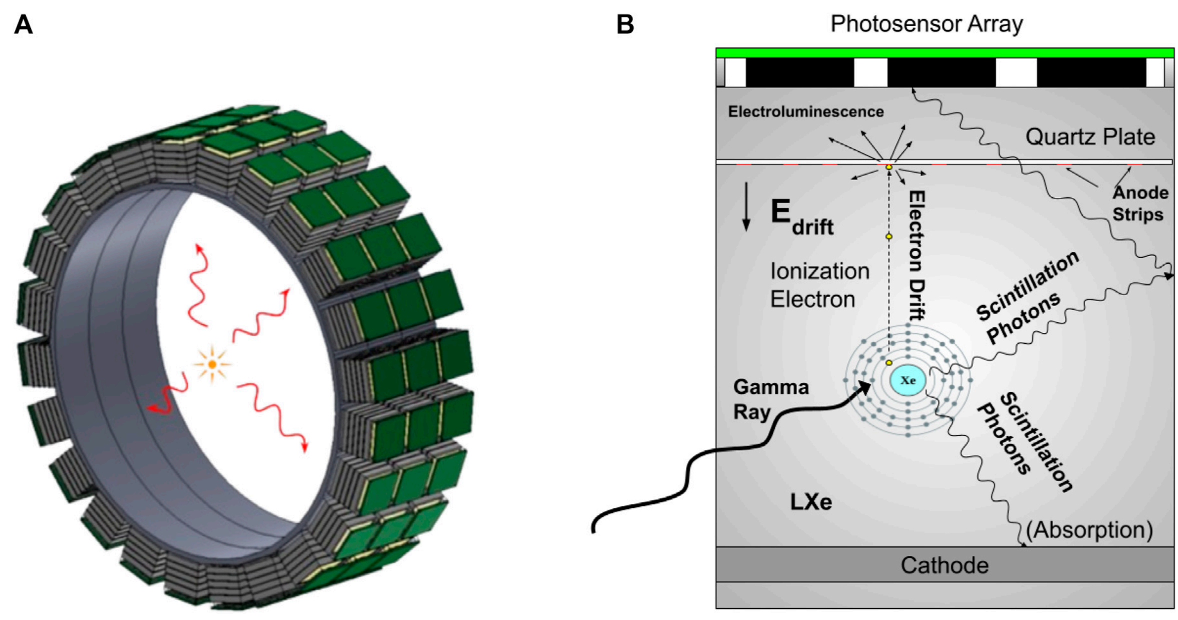

FIGURE 1
(A) Conceptual design of a LXe-based PET imaging system with concentric rings of LXe detectors detecting two back-to-back 511 keV gamma rays from a positron emission source. **(B)** The design principle of the individual LXe detector detects both prompt scintillation photons and delayed ionization signals through field-enhanced electroluminescence at the anode. The monolithic liquid xenon target enhances the light collection. The single-ended photo-sensors reduce the cost but at the same time are sufficient to provide sub-mm 3D spatial resolution.

SAES PS4-MT50-R used in XENON1T, to remove electronegative impurities to allow free drift of ionization electrons in the liquid. The detailed engineering design of these systems for the LXePET is out of the scope of this paper but we envision smaller scale systems will be needed to operate the LXePET detector, which in our design contains less than 100-kg of liquid xenon, compared to the ton-scale dark matter detector.

A design of the central part of our proposed PET imaging system with individual LXe detectors is shown in Figure 1A. The imaging system contains concentric rings of individual detectors (PET detectors) of about $5 \times 5 \times 5\,cm^3$, filled with liquid xenon as the gamma-ray detection medium. The LXe PET detector will detect both the prompt scintillation (S1) and delayed ionization signals through field-enhanced electroluminescence (S2) to enable high energy and position resolutions.

Field-enhanced electroluminescence in LXe was first demonstrated by Aprile et al. (2014) in a single-wire test chamber. Recent development has shown that stable operation on a large kg target can be performed in a single wire proportional scintillation counter (Qi et al., 2023) and time projection chamber (TPC) with thin wire anode (Tönnies et al., 2024). Here we follow the concept from (Breskin, 2022), which proposes several novel ways including the use of a micro-strip anode plate to generate electroluminescence in LXe, to design our PET detector, with its principle shown in Figure 1B. When a particle, such as the 511 keV gamma ray from the positron radioactive source, enters the liquid xenon medium, it deposits energy and produces scintillation photons (S1) and ionization electrons, which drift towards the anode plate under an electric field. A strong field near the strip on the anode converts these electrons into electroluminescence (S2). The same photo-sensor array, located right above the anode plane, detects both S1 and S2 to reconstruct the energy and position of the energy deposition.

We use SOLIDWORKS, a 3D CAD software, to create mechanical prototype design for the LXe PET detectors (Figure 2). This software helps with measurements and the general design of the PET detectors with Teflon walls containing the liquid xenon target in a $5 \times 5 \times 5\,cm^3$ detection volume. The size of the PET detector is chosen to efficiently detect the 511-keV gamma rays interacting in LXe while minimizing the PET detector numbers for system complication and cost. The highly reflective Teflon walls improve light detection (see Section 3.1), which is essential in determining the energy resolution. The detector is instrumented with electrodes and shaping rings to optimize the detection of ionization electrons (see Section 3.2. An array of photosensors detect both the primary scintillation and electroluminescence from ionization. The electroluminescence has similar spectrum range to the scintillation light from liquid xenon. The design uses 3×3 Hamamatsu S13371-6050CQ-02 silicon photomultipliers (SiPMs), each having a photon detection area about 144mm^2. The SiPMs feature both a compact mechanical structure and are capable of detecting the 175 nm vacuum ultra-violate (VUV) photons from LXe with a photon detection efficiency about 24%. It is worth to note that the MEG experiment used this type of SiPMs and observed UV-induced degradation Ieki et al. (2023). Given the EL light exposure rate in our PET design, long-term SiPM stability should be further investigated in an experimental setting. One notable instance of design oversight pertains to the distance between the anode and photo sensors, a critical parameter to position accuracy. Machine learning algorithms are developed (see Section 4) to investigate and optimize such a distance.

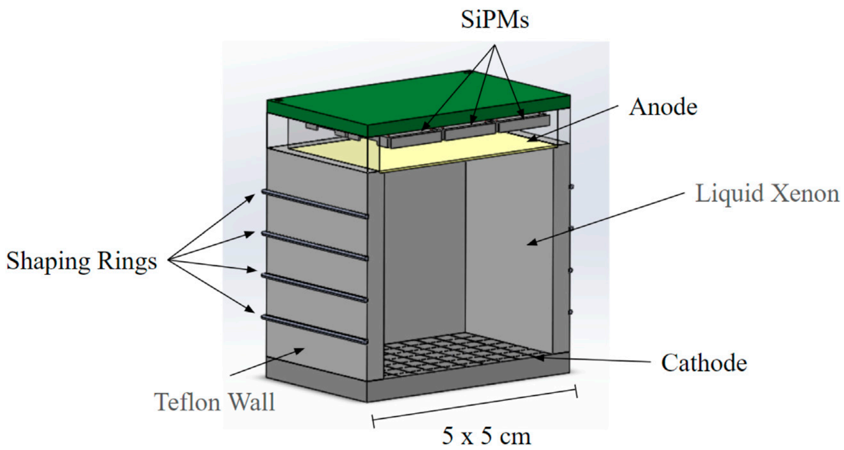

FIGURE 2
Mechanical design of the LXe detector for the PET detector, showing Teflon wall containing the bulk of $5 \times 5 \times 5\,cm^3$ liquid xenon inside. Stainless steel mesh serves as the cathode and an anode quartz plate, coated with thin metal strips, defines the ionization electron drift volume. Shaping rings are spaced to optimize the field uniformity. A 3×3 SiPM photosensors array is placed above the anode.

3 Signal detection and energy resolution

To validate the design, we use GEANT4 (Agostinelli et al., 2003), an open-source particle simulation software, to simulate particle trajectories and collect data, aiding in the design process. We implement our design in GEANT4 to trace light generated in the detector and detected by the SiPMs, comparing the light collection efficiency for different reflectivity of the Teflon wall. Additionally, we utilize COMSOL Multiphysics COMSOL Inc. (2024), a simulation software that aids in studying electromagnetism for generating electric fields. COMSOL enables us to examine electrode configurations and electric field uniformity which is crucial for ionization electron detection efficiency.

Specific pieces that went through multiple design iterations are shown. For example, the thickness of Teflon was important as we needed to factor in space for shaping rings as well as the rigidness of the cathode anode. Electric field simulations ultimately determined that this space should be created as uniform an electric field as possible. The stainless-steel mesh was important to allow for as much light to pass through as possible. Finally, we compared the pros and cons of adding SiPM sensors in a 2×2 versus 3×3. While a 2×2 SiPM sensor is more cost-efficient, a 3×3 SiPM sensor layout will enlarge the detector size to 5 by 5 cm, allowing the detector to have higher light collection efficiency and electric field uniformity.

3.1 Light collection efficiency

Simulated by GEANT4, scintillation photons (S1) produced by 511 keV gamma rays in liquid xenon are reflected by the Teflon wall, absorbed by surrounding materials or detected by the nine photo-sensors. Light collection efficiency is defined as the ratio between the number of photons reaching the photosensors and the number of scintillation photons produced at the gamma-ray interaction point. A higher light collection efficiency will improve the energy resolution of the PET detector, as studied in Section 3.3.

Figure 3 shows the light collection efficiency at four different heights in the PET detector. The collection efficiency is higher at a higher position in the detector due to the closer position to the photosensor. But they also show non-uniformity seen by the nine photosensors. The lower part of the detector shows better light collection uniformity. Teflon reflectivity in liquid xenon will affect the overall light collection efficiency in the detector. Measurements in the dark matter detector field show a high reflectivity of more than 97% Neves et al. (2017). We ran our simulation for reflectivity from 90% to 99%. An average efficiency of 78.2% is obtained in the entire volume with a 99% Teflon reflectivity. Reducing the reflectivity to 90% would result in a lower average light collection down to 56.0%.

3.2 Electron detection efficiency

When ionization electrons are produced inside the detector, they will follow the electric field, also called as drift field, generated by the anode and cathode. We used the COMSOL Multiphysics package to simulate the electric field to study the electron detection efficiency. The dielectric properties of Teflon ($\varepsilon_r \approx 2.1$) and LXe ($\varepsilon_r \approx 1.9$) were included in simulations to ensure accurate electric field modeling. The drift field can be generated by applying either negative voltage on the cathode or positive voltage on the anode. Both voltages can be introduced to liquid xenon with high voltage feed-throughs rated for vacuum systems. The anode also requires a high voltage in order to produce the very high field (400 V/cm) around the thin metal strips to generate electroluminescence. We simplify the design by introducing +5 kV on the anode to produce both the drift field and electroluminescence field while setting the cathode at ground. To maintain a uniform drift field in the LXe volume, we added four shaping rings, which will be connected with resistors between each and between them and the anode and cathode. Figure 4 shows the simulated electric field in the PET

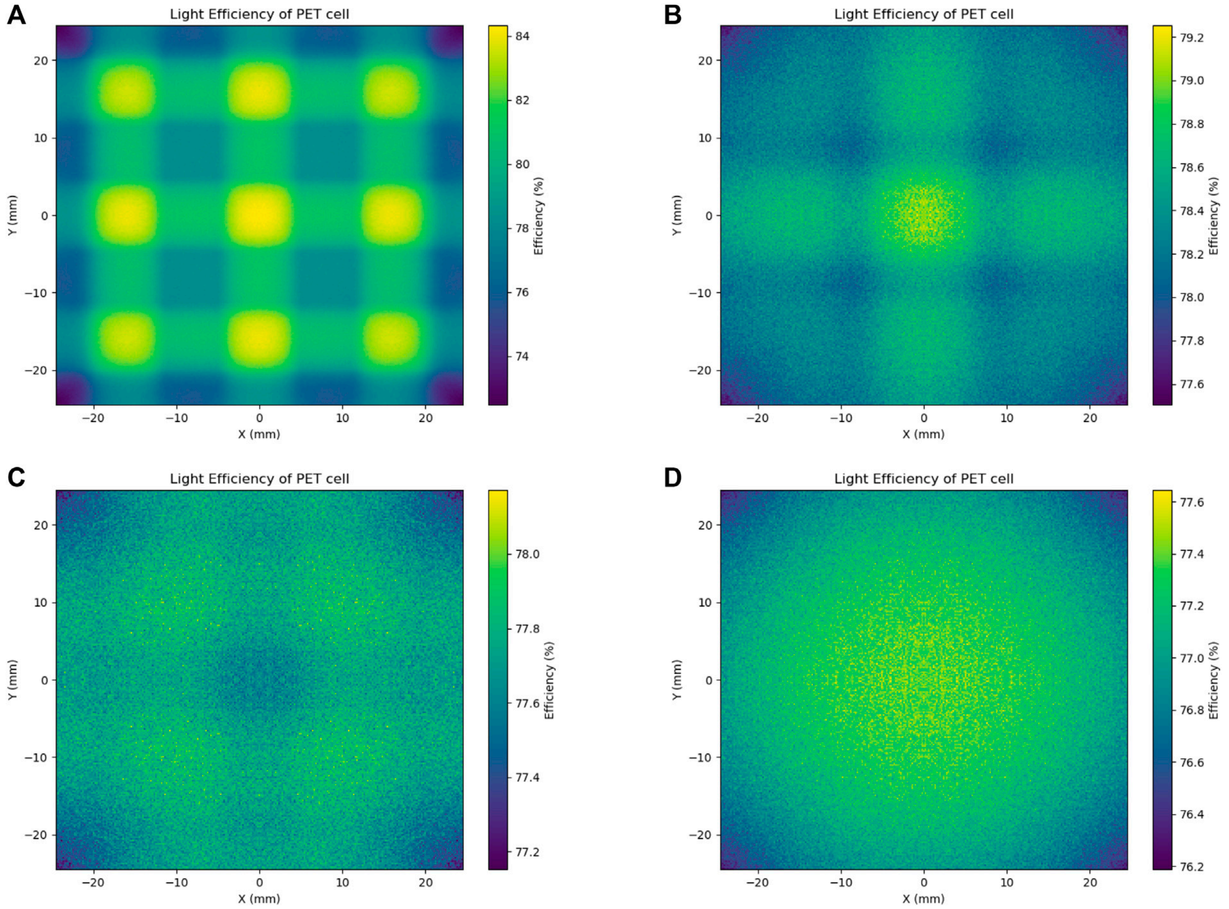

FIGURE 3
Light collection efficiency at four different heights **(A)**: 1 mm, **(B)**: 15 mm, **(C)**: 25 mm, **(D)**: 45 mm below the anode) in the PET detector. The Teflon wall reflectivity is set at 99% in this simulation.

detector. We found that without shaping rings, the electric field curves significantly in the detector, and about 5%–20% of the electrons drifting from the bottom near the walls will be lost from running into the walls. After adding four evenly distributed shaping rings with respective electric potentials calculated to create a uniform electric field, nearly 100% electrons from the bottom will be able to reach the anode, increasing the event detection efficiency.

The ionization electrons follow the electric field and drift towards the anode to create electroluminescence. Figure 5 shows a magnified region near the anode where the field strength becomes very high, with thin metal strips (5 μm in this simulation), allowing the generation of electroluminescence in liquid xenon Aprile et al. (2014). This anode structure allows most electrons to drift towards metal strips with electric potentials of 5 kV, where electroluminescence can be created in liquid xenon near the anode strips Martinez-Lema et al. (2024).

The simulated electric fields in the PET detector drift volume and near the anode show that ionization electrons can be detected with near 100% efficiency in the entire $5 \times 5 \times 5\,cm^3$ target volume and 5 kV on the anode is sufficient to produce the electroluminescence to be detected by the same SiPM array. This design requires no additional charge readout electronics.

3.3 Energy resolution

We integrate the electron and light detection efficiency with knowledge of energy reconstruction of a liquid xenon detector to investigate the energy resolution in such a detector for 511 keV gamma rays for PET imaging. The 511 keV gamma rays deposit energy in the PET detector by releasing primary scintillation light (S1) and ionization charges. The ionization charges drift along the field lines and create electroluminescence (S2) when entering the strong field near the anode. Detecting and combining S1 and S2 signals improves the energy resolution of the gamma-ray detection. Here we use fully photo-absorbed 511-keV gamma ray for a simplified simulation. Brief discussion about single/multiple scatters is presented in the last section and will be studied in the future.

The total energy of an event can be reconstructed using: $E = (S1/g_1 + S2/g_2) \cdot W$, where W is the average energy, about 13.6 eV, required to generate a photon or ionization electron in liquid xenon. g_1 and g_2 are gain factors related to S1 and S2 detection respectively, and they can be estimated based on our simulated light collection efficiency multiplied by the photon detection efficiency (PDE) of the SiPMs, approximately 24% according to the manufacturer's specification. For g_2, there is an additional factor of electroluminescence photon production, which is about 20 photons per

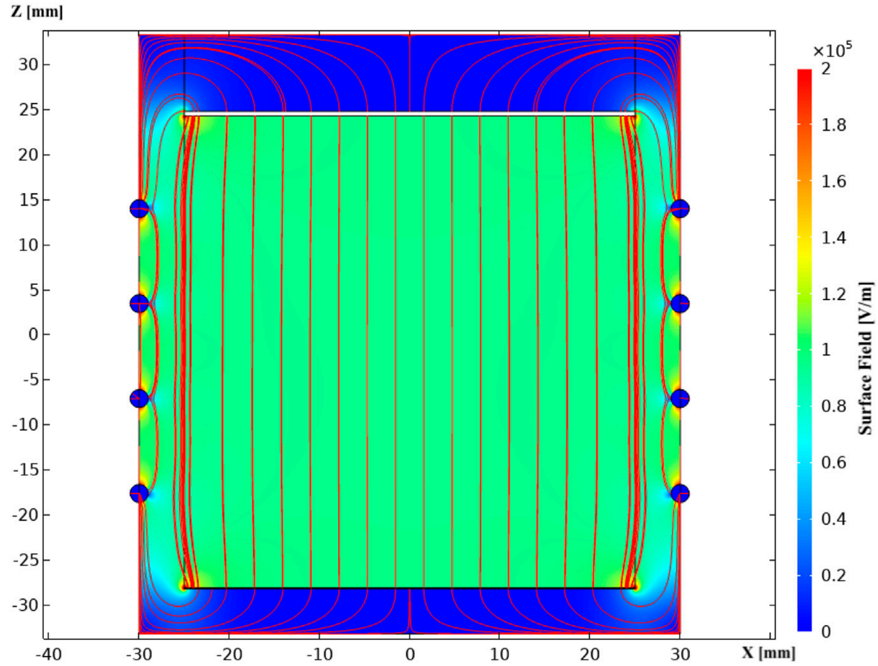

FIGURE 4
Simulation of the electric field in the PET detector showing the uniform field that will drift ionization electrons towards the anode. The shaping rings enhance the uniformity of the field, maximizing the sensitive target volume. In this simulation, 5-kV is applied to the anode (~+24 mm) and the cathode (~-28 mm) is set at ground. The top of the anode plate is grounded, limiting the field between the anode and top SiPM sensors to near zero. The field below the grounding cathode, where Teflon reflectors are located, is also close to zero.

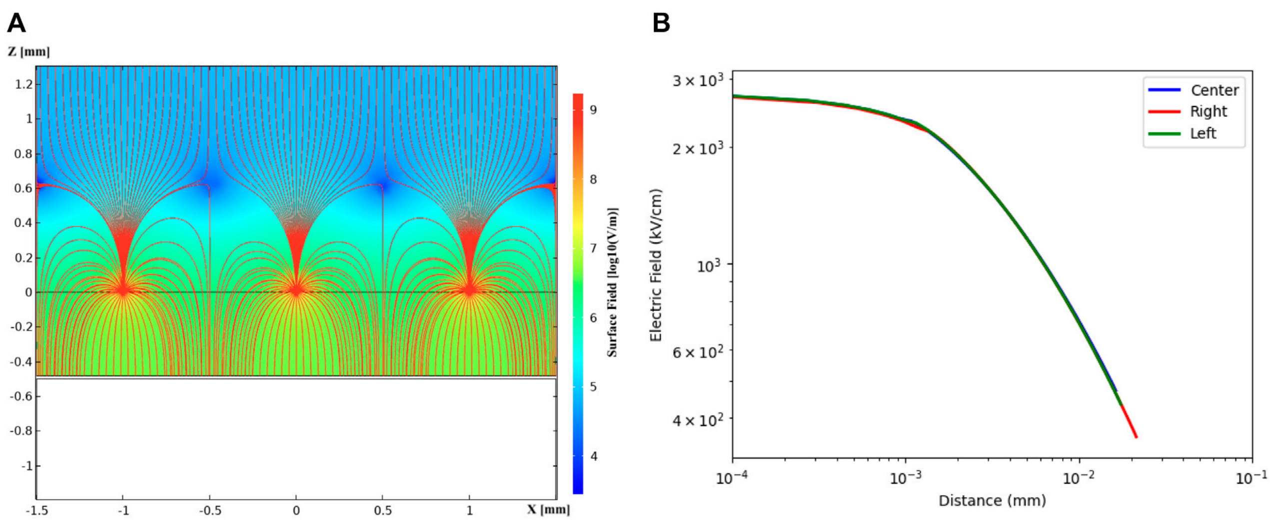

FIGURE 5
Simulation of the electric field near the anode region with the electrical potential set at +5 kV on the 5 μm wide and 0.1 μm thick metal strips of the anode **(A)** The solid lines are electric field lines from the cathode (50 mm above the anode, out of the figure) to the anode (Z = 0). The color represents the strength of the electric field in a unit of log10(V/m). **(B)** The electric field strength, on the central field lines in the simulated three anode strips, as a function of distance near the anode strips. The simulation shows a very strong field near the anode, exceeding the liquid xenon electroluminescence generation threshold of about 400 kV/cm Aprile et al. (2014) at 10 μm distance near the anode.

electron hitting the anode, according to Qi et al. (2023). Thus we obtain the g_1 and g_2 according to our simulated light and charge detection efficiencies in the previous section: $g_1 = 0.16 \pm 0.03$ photoelectron/photon (PE/photon) and $g_2 = 3.4 \pm 0.4$ photoelectron/electron (PE/electron). The error bars represent the uncertainty related to the Teflon reflectivity (90%–99%).

Finally, the energy resolution for 511-keV gamma rays in liquid xenon is studied using the Noble Element Simulation Toolkit

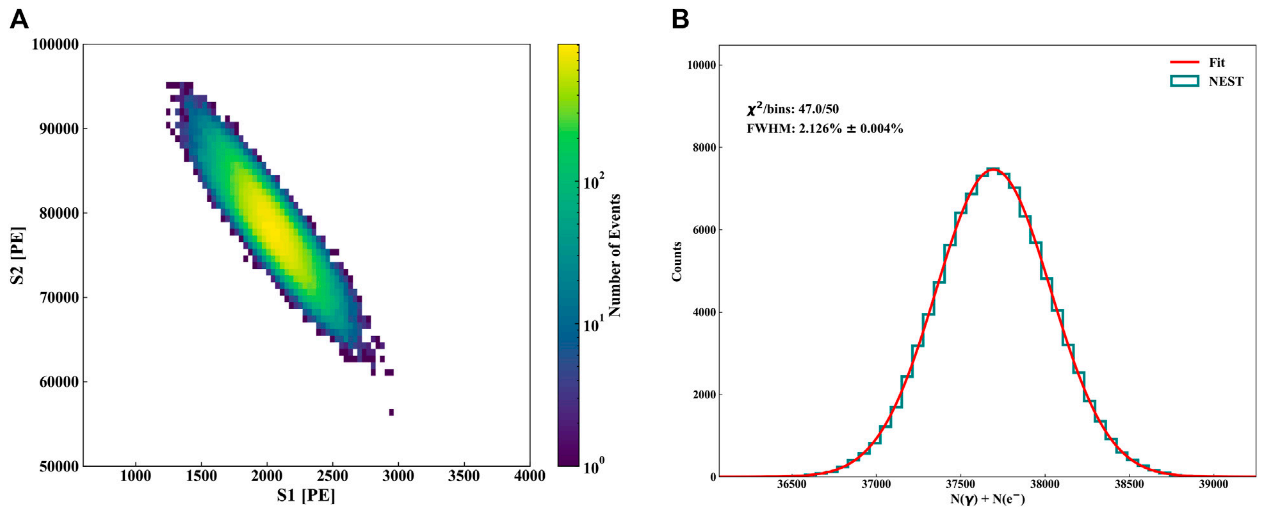

FIGURE 6
NEST-based simulation study for detecting 511-keV gamma rays in our proposed liquid xenon detector design with g_1 = 0.16 PE/photon and g_2 = 3.4 PE/electron **(A)** simulated detection of S1 and S2 in a unit of photoelectron (PE) detected by the SiPMs array. S1 and S2 represents the scintillation and ionization signals generated by the energy deposition of 511-keV gamma rays in liquid xenon. They show an anti-correlation feature, due to the recombination fluctuation in liquid xenon, as observed by the previous experiments Anton et al. (2020); Aprile et al. (2020) **(B)** The energy spectrum combining the scintillation and ionization signals for the photo-absorbed 511-keV gamma rays in liquid xenon. A Gaussian fit reveals a FWHM resolution of 2.1%.

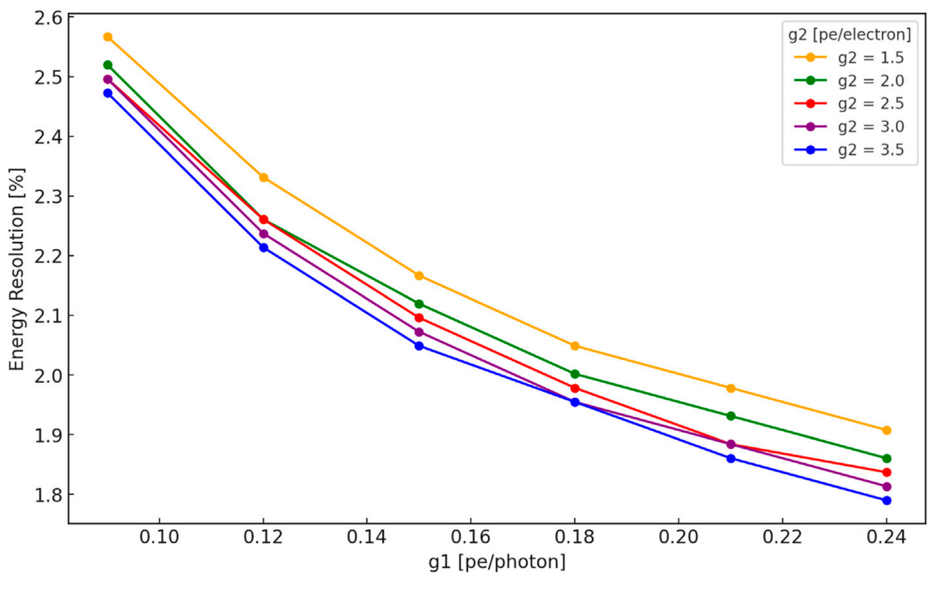

FIGURE 7
NEST-based simulation study of liquid xenon energy resolution (FWHM) for 511-keV gamma rays at different light (g_1) and charge (g_2) detection efficiencies.

(NEST) (Szydagis et al., 2011; Szydagis et al., 2022), shown in Figure 6. Based on the g_1 and g_2 values obtained from Section 3.1 and Section 3.2, we estimate that the PET detector can achieve a FWHM energy resolution of 2.1%. This is an improvement of about a factor of 5 compared to the current PET detector technology with scintillation crystals. The resolution can be further improved with a higher g_1 or g_2 values, according to our simulated results for different g_1 and g_2 values in Figure 7.

4 Position reconstruction and spatial resolution

In our proposed LXe PET detector, the gamma rays depositing energy in the monolithic LXe target produce a prompt scintillation signal (S1), followed by a delayed ionization-induced electroluminescence signal (S2). The time difference between the S1 and S2 provides the depth-of-interaction (DOI) information with

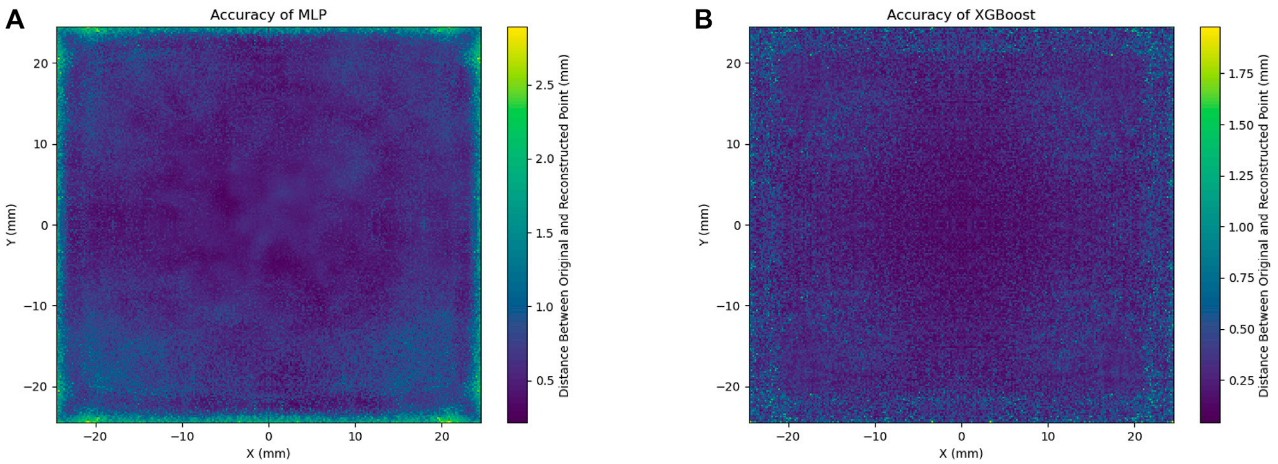

FIGURE 8
"Accuracy" of reconstructed positions at different X&Y in the PET detector for the MLP **(A)** and XGBoost **(B)** methods.

a sub-mm spatial resolution (Tönnies et al., 2024). The S2 light pattern, collected by the 3 × 3 photosensor array above the anode, reconstructs the horizontal (X&Y) positions. We investigate two methods of reconstructing the gamma-ray's XY position in the LXe PET detector.

Both methods consist of training machine learning models. The first method constructs a multilayer perceptron (MLP) model (Taud and Mas, 2018), while the second constructs a model using XGBoost (Chen and Guestrin, 2016). To train each model, we take the nine numbers corresponding to the number of photons each SiPM detected, feed it to the model, and then evaluate model performance based on how close the reconstructed gammy ray position was to the original position.

To gather the data needed to perform and evaluate these methods, the PET detector was constructed in GEANT4, and the generation of the photons from a single point due to the gamma-ray interacting with the PET detector was simulated. Due to the symmetrical nature of the PET detector, points in a single quadrant of the entire sensitive target, with a separation of 0.2 mm between each point, were equally spaced and generated in the PET detector. The generated data was then reflected across the axes to get the data for the other three quadrants. We vary the anode distance relative to the SiPM array in the PET detector and find the best position reconstruction results that can be achieved is at an anode distance about 10 mm below the SiPM array. In the following, we present results for an anode distance 10 mm below the SiPM array.

We define "accuracy" as the relative distance between the reconstructed position and the original position. The reconstructed position accuracy at different X&Y positions is shown in Figure 8 for the two methods. Both methods achieve an average accuracy value around zero, indicating no systematic bias. The MLP model shows a wider distribution (Figure 9) than the XGBoost model. The MLP method performs better when the gamma-ray position is near the center of the PET detector, and poorly near the edges and corners. The XGBoost model performs well in the entire target volume.

Plotting the difference in positions, for both X&Y, between the original and reconstructed positions reveals a distribution centered around zero for the MLP method, with a wider base corresponding to the edges and corners of the cell, as shown in Figure 9. For the XGBoost method, there is Gaussian-like distribution centered at zero. Fitting the distribution with a Gaussian function reveals a FWHM resolution of 0.56 mm.

From Figure 8, we can see poorer position reconstruction near the edge of the detector. This is due to the increased inaccuracies of the models near the edges. We performed further study by removing points within 5 mm of the edge of the PET detector, and then the models were trained and tested on all the remaining points. Removing the 5-mm from the edge of detector reduces the sensitive target to about 67% of the total volume. While the MLP method's shows slightly better performance, it still shows a wider base (Figure 10, left). The XGBoost model achieves an improved FWHM position resolution to 0.34 mm in the central volume.

Although there are various methods for using machine learning to reconstruct positions and optimize target volume selection, the sub-millimeter position sensitivity of the proposed LXe PET design offers the potential to enhance the overall position sensitivity of a complete PET system. This improvement could lead to a reduction in the radioactive dose required for patients.

5 Discussion and future work

Our study highlights the potential of liquid xenon (LXe)-based detectors to significantly enhance the performance of Positron Emission Tomography (PET) imaging systems. By combining scintillation and ionization energy detection, the proposed design overcomes the limitations of traditional scintillation crystal-based PET systems. Based on our simulations, the design achieves an energy resolution of approximately 2.1% (FWHM), representing a five-fold improvement over current PET technology. Additionally, sub-millimeter position resolution can be attained for gamma-ray interaction points using machine learning models. The LXePET will use mainly the single-scatter (SS) photo-absorbed 511-keV gamma events to reconstruct the position of the radioactive source. The gamma rays can make Compton multiple scatterings on the cryostat and the liquid xenon target itself. Selecting SS from MS events thus

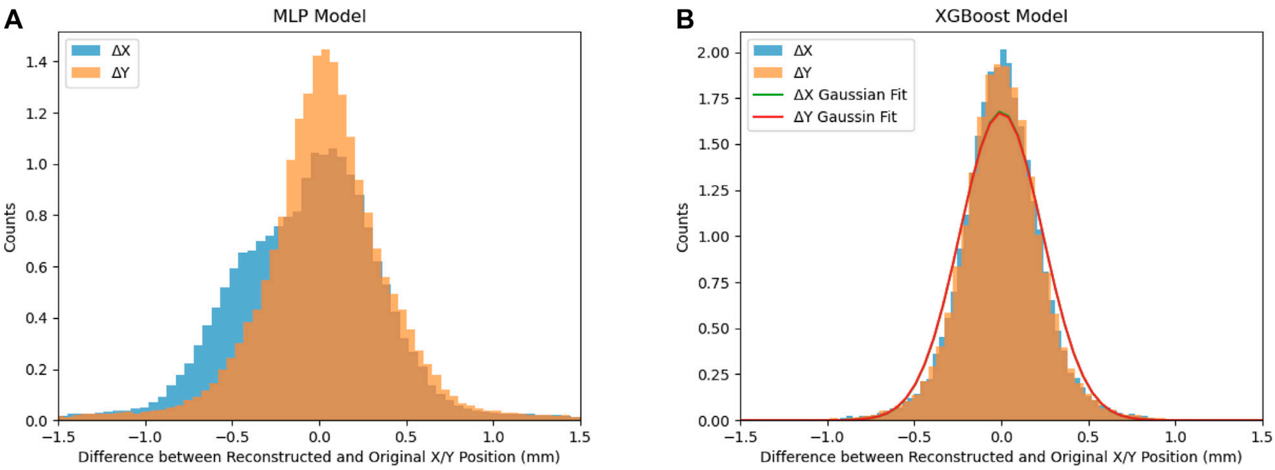

FIGURE 9
Relative distances for both X and Y between the original and reconstructed points for the MLP **(A)** and XGBoost **(B)** methods in the entire target volume. The MLP method shows a distribution centered near zero, but the wider base corresponds to the inaccurate reconstructed positions near the edge and corners. The XGBoost performs much better and shows Gaussian-like distributions centered at zero, and FWHM position resolutions of 0.56-mm.

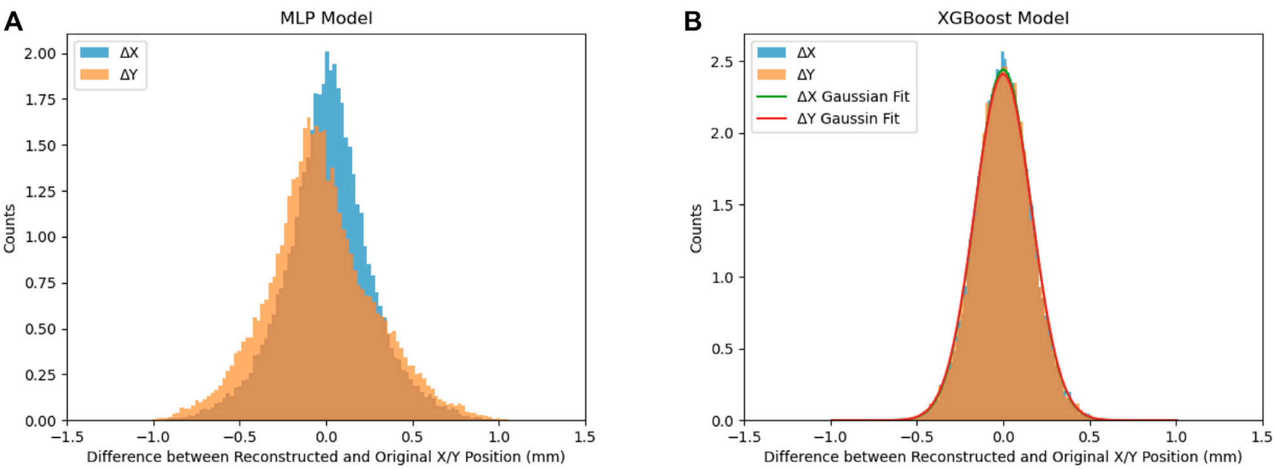

FIGURE 10
Relative distances for both X and Y between the original and reconstructed points for the MLP **(A)** and XGBoost **(B)** methods, in the smaller (5-mm removed from all edges) selected target volume. The MLP method still shows a wider base. The XGBoost performs better and shows Gaussian distributions centered at zero and FWHM position resolutions of 0.34-mm for both X and Y.

will be the key for enhanced performance. We ran a Geant4 simulation of 511-keV gamma rays interacting in the LXePET and used the simulated spatial resolution (0.56 mm FWHM) for identifying the SS/MS events. Figure 11 shows the SS and MS events identified in the LXe target. In the 2.1% (FWHM) window around the 511-keV peak. The SS event accounts for about 44% of the events detected. While the pure SS photo-absorbed events will improve the time-of-flight reconstruction precision, the first interaction of fully contained multiple scattering events can be used for time-of-flight and energy reconstruction. The multiple Compton scattering events can be used as well to reconstruct source positions, as used in the XEMIS2 detector for medical imaging Manzano et al. (2018).

One consideration of using both scintillation and ionization signals for LXePET is the event pile-up. At the design field of 1 kV/cm, the electron drift speed can reach about 2 mm/μs Albert et al. (2017), giving a maximum drift time (dt_{max}) about 25 μs across the 5-cm distance from the cathode to anode. The probability of two events piling up in the same dt_{max} window can be estimated by multiplying the event rate. The pile-up probability is ~13% for an event rate of 5 kHz. Such an event rate would be reasonable to operate the LXePET detector in both scintillation and ionization mode to identify enough good events without pile-ups. Event selections, such as selecting events in the 511-keV energy window and pairing S1 and S2 events with their energy information to identify separate events, will further suppress the

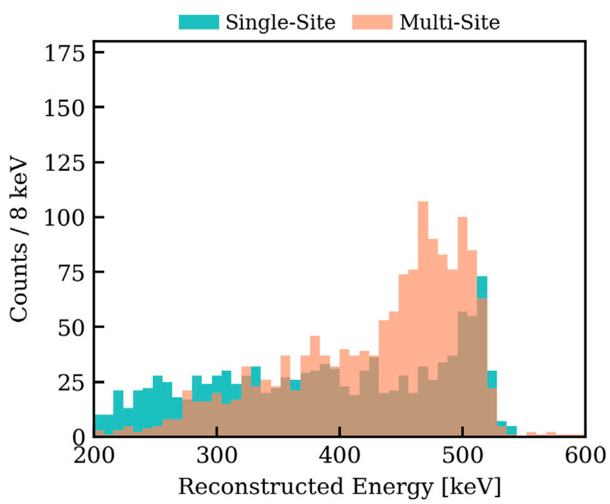

FIGURE 11
Single-site and multiple-site events identified from a Geant4 simulation of 511-keV gamma rays entering the LXe target volume from outside a stainless steel cryostat. The selection of SS/MS events is based on a spatial resolution of 0.56-mm in the whole volume, as studied in the previous section. The SS/MS event ratio is about 78% in the FWHM energy window around the 511-keV peak, i.e., SS/total is 44%.

pile-up probability. Assuming the distance between the single LXePET cell window (5×5 cm^2) and the center of the ring (Figure 1A) of 20-cm, the corresponding radiation dosage is estimated to be around 1 MBq to produce 5 kHz events in the cell. The image reconstruction capability of the whole LXePET detector, taking into account the low radiation dosage, SS/MS event reconstruction and background events, will be investigated in a future study.

In our design, the 5-cm thick liquid xenon (LXe) detector, with a density of 2.89 g/cm^3; and an attenuation length of 3.7 cm (Gomez-Cadenas et al., 2016) for 511-keV gamma rays, can achieve an estimated detection efficiency of 74%. This is comparable to similar thickness NaI(Tl) detector but is slightly lower than LYSO/BGO crystals with more than 90% efficiency for typical PET detector thicknesses of 2-cm. Increasing the thickness of the LXe detector will increase the pileup rate but also the cost of material. However, the high position and energy resolutions effectively reduces background events in the 511-keV gamma-ray energy window, thereby lowering the required patient exposure time and radiation dose. The enhanced position resolution further improves the accuracy of reconstructed positions within the patient's body. The efficiency of our monolithic LXe target design not only provides more precise positioning and accuracy but also simplifies the mechanics and reduces costs if implemented in medical imaging systems.

While our simulated results are promising, this work only presents the potential of a LXeTPC for PET applications. The practical implementation of a LXe PET detector still needs to be demonstrated. Although the detection of liquid xenon scintillation light with SiPMs has been successfully achieved in several particle physics experiments, the detection of ionization-induced electroluminescence in liquid xenon has only been demonstrated in small-scale, table-top prototypes (Qi et al., 2023; Martinez-Lema et al., 2024; Qi et al., 2025). The reliability and performance of the proposed LXe PET detector must be validated and optimized for real-world applications, with experimental efforts required to address any unforeseen challenges that may arise during the transition from simulation to laboratory testing.

Data availability statement

The original contributions presented in the study are included in the article/supplementary material, further inquiries can be directed to the corresponding author.

Author contributions

AB: Conceptualization, Data curation, Formal Analysis, Investigation, Methodology, Software, Validation, Visualization, Writing – original draft, Writing – review and editing. JF: Conceptualization, Data curation, Formal Analysis, Investigation, Methodology, Software, Validation, Visualization, Writing – original draft, Writing – review and editing. MN: Conceptualization, Data curation, Formal Analysis, Investigation, Methodology, Software, Validation, Visualization, Writing – original draft, Writing – review and editing. MZ: Conceptualization, Data curation, Formal Analysis, Investigation, Methodology, Software, Validation, Visualization, Writing – original draft, Writing – review and editing.

Funding

The author(s) declare that no financial support was received for the research and/or publication of this article.

Acknowledgments

The authors would like to thank Aobo Li for suggestion of using the XGBoost model for position reconstruction.

Conflict of interest

The authors declare that the research was conducted in the absence of any commercial or financial relationships that could be construed as a potential conflict of interest.

Publisher's note

All claims expressed in this article are solely those of the authors and do not necessarily represent those of their affiliated organizations, or those of the publisher, the editors and the reviewers. Any product that may be evaluated in this article, or claim that may be made by its manufacturer, is not guaranteed or endorsed by the publisher.

References

Agostinelli, S., Allison, J., Amako, K., Apostolakis, J., Araujo, H., Arce, P., et al. (2003). GEANT4 - a simulation Toolkit. *Nucl. Instrum. Methods Phys. Res. Sect. A Accel. Spectrom. Detect. Assoc. Equip.* 506, 250–303. doi:10.1016/S0168-9002(03)01368-8

Alauddin, M. M. (2012). Positron emission tomography (pet) imaging with (18)f-based radiotracers. *Am. J. Nucl. Med. Mol. Imaging* 2, 55–76. Epub 2011 Dec 15.

Albert, J. B., Barbeau, P. S., Beck, D., Belov, V., Breidenbach, M., Brunner, T., et al. (2017). Measurement of the drift velocity and transverse diffusion of electrons in liquid xenon with the EXO-200 detector. *Phys. Rev. C* 95, 025502. doi:10.1103/PhysRevC.95.025502

Amaudruz, P., Bryman, D., Kurchaninov, L., Lu, P., Marshall, C., Martin, J., et al. (2009). Simultaneous reconstruction of scintillation light and ionization charge produced by 511kev photons in liquid xenon: potential application to pet. *Nucl. Instrum. Methods Phys. Res. Sect. A Accel. Spectrom. Detect. Assoc. Equip.* 607, 668–676. doi:10.1016/j.nima.2009.06.036

Anton, G., Badhrees, I., Barbeau, P. S., Beck, D., Belov, V., Bhatta, T., et al. (2020). Measurement of the scintillation and ionization response of liquid xenon at MeV energies in the EXO-200 experiment. *Phys. Rev. C* 101, 065501. doi:10.1103/PhysRevC.101.065501

Aprile, E., Aalbers, J., Agostini, F., Alfonsi, M., Althueser, L., Amaro, F. D., et al. (2020). Energy resolution and linearity of XENON1T in the MeV energy range. *Eur. Phys. J. C* 80, 785. doi:10.1140/epjc/s10052-020-8284-0

Aprile, E., Aalbers, J., Agostini, F., Alfonsi, M., Amaro, F. D., Anthony, M., et al. (2017). The XENON1T dark matter experiment. *Eur. Phys. J. C* 77, 881. doi:10.1140/epjc/s10052-017-5326-3

Aprile, E., Contreras, H., Goetzke, L. W., Fernandez, A. J. M., Messina, M., Naganoma, J., et al. (2014). Measurements of proportional scintillation and electron multiplication in liquid xenon using thin wires. *JINST* 9, P11012. doi:10.1088/1748-0221/9/11/P11012

Berg, E., and Cherry, S. R. (2018). Innovations in instrumentation for positron emission tomography. *Seminars Nucl. Med.* 48 (Instrumentation), 311–331. doi:10.1053/j.semnuclmed.2018.02.006

Breskin, A. (2022). Novel electron and photon recording concepts in noble-liquid detectors. *J. Instrum.* 17, P08002. doi:10.1088/1748-0221/17/08/P08002

Chen, T., and Guestrin, C. (2016). "Xgboost: a scalable tree boosting system," in Proceedings of the 22nd ACM SIGKDD International Conference on Knowledge Discovery and Data Mining (ACM) (KDD '16). *New York, NY, United States: Association for Computing Machinery (ACM).* doi:10.1145/2939672.2939785

Chepel, V., Solovov, V., Van Der Marel, J., Lopes, M., Crespo, P., Janeiro, L., et al. (1999). The liquid xenon detector for pet: recent results. *IEEE Trans. Nucl. Sci.* 46, 1038–1044. doi:10.1109/23.790822

COMSOL Inc. (2024). Comsol multiphysics user guide

Doke, T., Kikuchi, J., and Nishikido, F. (2006). Time-of-flight positron emission tomography using liquid xenon scintillation. *Nucl. Instrum. Methods Phys. Res. Sect. A Accel. Spectrom. Detect. Assoc. Equip.* 569, 863–871. doi:10.1016/j.nima.2006.07.067

Giboni, K., Aprile, E., Doke, T., Suzuki, S., Fernandes, L. M. P., Lopes, J. A. M., et al. (2007). Compton positron emission tomography with a liquid xenon time projection chamber. *J. Instrum.* 2, P10001. doi:10.1088/1748-0221/2/10/P10001

Gomez-Cadenas, J., Benlloch-Rodríguez, J. m., Ferrario, P., Monrabal, F., Rodríguez, J., and Toledo, J. (2016). Investigation of the coincidence resolving time performance of a pet scanner based on liquid xenon: a Monte Carlo study. *J. Instrum.* 11, P09011. doi:10.1088/1748-0221/11/09/p09011

Ieki, K., Iwamoto, T., Kobayashi, S., Mori, T., Ogawa, S., Onda, R., et al. (2023). Study on degradation of VUV-sensitivity of MPPC for liquid xenon scintillation detector by radiation damage in MEG II experiment. *Nucl. Instrum. Methods Phys. Res. Sect. A Accel. Spectrom. Detect. Assoc. Equip.* 1053, 168365. doi:10.1016/j.nima.2023.168365

Manzano, L. G., Abaline, J. M., Acounis, S., Beaupère, N., Beney, J. L., Bert, J., et al. (2018). XEMIS2: a liquid xenon detector for small animal medical imaging. *Nucl. Instrum. Meth. A* 912, 329–332. doi:10.1016/j.nima.2017.12.022

Martinez-Lema, G., Chepel, V., Roy, A., and Breskin, A. (2024). First observation of liquid xenon electroluminescence with a MicroStrip Plate. *JINST* 19, P02037. doi:10.1088/1748-0221/19/02/P02037

Miceli, A., Amaudruz, P., Benard, F., Bryman, D. A., Kurchaninov, L., Martin, J. P., et al. (2011). Liquid xenon detectors for positron emission tomography. *J. Phys. Conf. Ser.* 312, 062006. doi:10.1088/1742-6596/312/6/062006

Mordor Intelligence (2024). Positron emission tomography (PET) market size.

Neves, F., Lindote, A., Morozov, A., Solovov, V., Silva, C., Bras, P., et al. (2017). Measurement of the absolute reflectance of polytetrafluoroethylene (PTFE) immersed in liquid xenon. *JINST* 12, P01017. doi:10.1088/1748-0221/12/01/P01017

Pereira, G., Silva, C., Solovov, V., and on behalf of the LZ collaboration (2023). Energy resolution of the lz detector for high-energy electronic recoils. *J. Instrum.* 18, C04007. doi:10.1088/1748-0221/18/04/C04007

Qi, J., Hood, N., Kopec, A., Ma, Y., Xu, H., Zhong, M., et al. (2023). Low energy electronic recoils and single electron detection with a liquid xenon proportional scintillation counter. *J. Instrum.* 18, P07027. doi:10.1088/1748-0221/18/07/P07027

Qi, J., Xu, H., Ma, Y., Liu, Y., and Ni, K. (2025). Feasibility of liquid-phase xenon proportional scintillation for low-energy physics. *Phys. Rev. D.* 111, 012005. doi:10.1103/PhysRevD.111.012005

Romo-Luque, C. (2020). PETALO: time-of-Flight PET with liquid xenon. *Nucl. Instrum. Methods Phys. Res. Sect. A Accel. Spectrom. Detect. Assoc. Equip.* 958, 162397. doi:10.1016/j.nima.2019.162397

Szydagis, M., Balajthy, J., Block, G. A., Brodsky, J. P., Brown, E., Cutter, J. E., et al. (2025). A review of NEST models for liquid xenon and an exhaustive comparison with other approaches. *Front. Detect. Sci. Technol.* 2. doi:10.3389/fdest.2024.1480975

Szydagis, M., Barry, N., Kazkaz, K., Mock, J., Stolp, D., Sweany, M., et al. (2011). Nest: a comprehensive model for scintillation yield in liquid xenon. *J. Instrum.* 6, P10002. doi:10.1088/1748-0221/6/10/p10002

Taud, H., and Mas, J.-F. (2018). Multilayer perceptron (mlp). *Lect. Notes Geoinformation Cartogr.*, 451–455. doi:10.1007/978-3-319-60801-3_27

Tönnies, F., Brown, A., Kiyim, B., Kuger, F., Lindemann, S., Meinhardt, P., et al. (2024). Proportional scintillation in liquid xenon: demonstration in a single-phase liquid-only time projection chamber

Vallabhajosula, S. (2023). *Radioactivity detection: PET and SPECT scanners*. Cham: Springer International Publishing, 63–86. doi:10.1007/978-3-031-23205-3_5